Nonlinear Dyn (2023) 111:15591–15612
https://doi.org/10.1007/s11071-023-08633-1

ORIGINAL PAPER

Spatio-temporal dynamics of an SIS model with nonlinear incidence and nonlocal disease transmission

Dhiraj Kumar Das · S. Ghorai · Malay Banerjee

Received: 6 March 2023 / Accepted: 28 May 2023 / Published online: 19 June 2023

Abstract Investigation of the spatio-temporal patterns exhibited by infected communities sharing the same spatial region is the focus of many researchers. Typically, an individual's susceptibility is substantially connected with the distance from nearby affected persons. Such a disease propagation mechanism is called the nonlocal infection which is primarily modeled with a kernel function K, whose support determines the range of the nonlocal infection area. In our current study, a susceptible–infected–susceptible-type epidemic model is analyzed considering the nonlinear disease incidence rate which is further extended to incorporate the nonlocal disease transmission and random movement of the individuals. Complete bifurcation characteristics of the associated temporal model include the saddle-node, subcritical Hopf, and homoclinic bifurcations. Our primary emphasis is to investigate the formation of a wide variety of spatio-temporal patterns that include stationary, quasi-periodic, periodic, and chaotic patterns, among others. Comparisons have been made between the spatio-temporal dynamics of the local and nonlocal disease transmission models. It is observed that the nonlocal disease transmission expands the parametric domain (referred to as Hopf and stable domains) on which the system possesses oscillatory and spatially homogeneous solutions. As a result, the spatially heterogeneous stationary solutions (referred to as Turing patterns) of the local system turn into irregular oscillatory solutions or spatially homogeneous solutions whenever the nonlocal extent of the disease transmission gradually increases. Also, the increased range of nonlocal infections reduces the number of stationary patches. In addition, the system exhibits "long transient" dynamics when the dispersal rate of the population tends to the Turing threshold. Exhaustive numerical simulations have been carried out to illustrate the wide range of spatio-temporal patterns displayed by the system in the presence and absence of nonlocal terms.

Keywords SIS epidemic model · Nonlocal infection · Spatio-temporal dynamics · Turing instability · Transient dynamics

D. K. Das (✉) · S. Ghorai · M. Banerjee
Department of Mathematics and Statistics, Indian Institute of Technology Kanpur, Kanpur, Uttar Pradesh 208016, India
e-mail: dhirajkd@iitk.ac.in

S. Ghorai
e-mail: sghorai@iitk.ac.in

M. Banerjee
e-mail: malayb@iitk.ac.in

1 Introduction

Analysis of the spread of communicable diseases is crucial to understand the underlying transmission mechanism of the disease. The elementary mathematical setup for this type of investigation is almost a century old and was framed by Kermack and McKendrick in 1927 [1]. They compartmentalized the total community into three disjoint sets according to individ-

ual clinical status namely susceptible, infected, and recovered. The interactions among the compartments followed by switching individual's clinical stage were described by coupled differential equations known as the SIR-epidemic model. After this paradigmatic work, several epidemic models were proposed and analyzed by numerous researchers [2–4]. The outcomes of these models are often useful in disease prevention, control, prediction, and other public health welfare.

The compartmental epidemic models come in a variety of forms depending upon the characteristics of the transmissible diseases. In particular, the number of compartments in an epidemic model is equal to the distinct clinically identifiable stages of the disease. For example, the SIR-type epidemic models are suitable to describe the disease in which individuals acquire immunity after a successful recovery. The SEIR-type epidemic models assume an exposed compartment E to represent the incubation stage where an individual is infected but not yet infectious. In addition, more complicated compartmental structures are possible which include vaccination, quarantine, hospitalization, different level of infectious stages, etc. A systematic formulation of the different types of epidemic models can be found in [5–7]. In this study, we consider an SIS-type epidemic model assuming that the transmissible disease does not confer immunity after recovery. This assumption confines the system to two compartments which can be used to study the transmission dynamics of many infectious diseases in humans and animals. Moreover, the simplest nature of the SIS-type models is favorable for mathematical analysis in reaction–diffusion setup.

In modeling the transmission of infectious diseases, the adopted per-capita disease incidence rate plays a central role in determining the dynamic behavior of the entire system. Most of the existing literature is based on bilinear-type incidence rate βSI, where S and I denote the densities of the susceptible and infectious present in a population with constant disease transmission rate $\beta > 0$. It relies on the linear interaction assumption between the S and I populations. However, this assumption may not be realistic or may be inefficient in mirroring disease transmission mechanisms when the population undergoes saturation effect or behavioral responses to avoid the risk of infections. Hence, some researchers proposed epidemic models taking into account the nonlinear disease incidence rates of various forms to address diverse complexities involved in disease transmission [8,9]. A general form of these kinds of incidence rates may be described by $\beta g(I)S$, where $g(.)$ is a continuous real-valued function. A wide range of qualitative differences in the dynamical characteristics is reported in the studies of epidemic models with nonlinear incidence rates compared to their bilinear counterparts. Epidemic models with bilinear-type incidence rates exhibit classical patterns in which the disease eradication is confirmed by monitoring a threshold value called basic reproduction number [10]. However, periodic solutions appear through Hopf bifurcation in models with nonlinear incidence rates and persistence of multiple endemic equilibria turns the system into multistable in nature [11]. Therefore, the presence of nonlinearity in disease incidence rates results in complexity in the qualitative dynamics of the system which causes more challenges and less predictability in preventing disease transmission.

The influence of the spatial mobility of two interacting communities on the spatial distribution of the population is widely investigated using reaction–diffusion equations [12,13]. The diffusion-driven instability, which is also known as Turing instability, is often used to explain various patterns exhibited by interacting populations in their natural habitat [14–17]. Further, the interplay between the susceptible and infected individuals in a community or species suffering from a contagious disease is conditionally similar to prey–predator interaction [18]. Therefore, to investigate the spatial heterogeneity many theoretical epidemiologists extended the temporal epidemic models into reaction–diffusion system by simply introducing a diffusion term [19–21]. Reaction–diffusion systems representing epidemic models exhibit spatio-temporal patterns [22,23] and traveling wave solutions [24–27]. A spatio-temporal pattern represents the distribution of the population both along space and time, whereas a traveling wave represents the transition of infection from one location to another. Our primary objective in this study is to explore the spatio-temporal patterns. A systematic review of the patterns exhibited by epidemic models can be found in [22].

In spite of the functional similarity in addressing the disease incidence rate and predation, there are many fundamental differences between these two mechanisms. Thus, special treatment is required to study the interaction both in mathematical epidemiology and eco-epidemiology [18]. However, very few attempts have been made to address this important issue. An

essential difference between these two mechanisms is the spatial location of the interacting individuals from different compartments. In particular, both the prey and predator must be present at the same spatial location for predation. On the other hand, an infectious individual can infect a distant susceptible individual when the causative agent of the disease can flow by air, water, or through any other communicable media. Therefore, it is reasonable to assume that the transmission of diseases is a nonlocal mechanism. Interaction or coupling between individuals present at different spatial locations allows the infection to spread to a wider range and acts to synchronize the epidemic dynamics. This type of behavior can be captured in an epidemic model by introducing a transmission kernel, K, which modifies the disease incidence rate and is a function of the distance between two individuals [5,27,28]. In particular, the modified incidence rate for a bounded interval Ω in one-dimensional space is given by

$$\lambda(x,t;I) = \beta \int_{\Omega} I(y,t)K(x-y)\mathrm{d}y,$$

which models the total transmission force exerted at the spatial location x at time t from other points y located in Ω. Here, β denotes the transmission rate of the disease. The transmission risk is expected to reduce as the spatial distance $|x-y|$ between the susceptible and infected individuals increases which must be an inherent feature of the transmission kernel K. Typically, K is a compactly supported probability density function on $\mathbb{R}$ and $K(x-y)$ weighs the contribution of an infected at a spatial location y toward infecting a susceptible individual at the location x. This modifies the system of ordinary differential equations to a system of integro-differential equations (IDEs).

In our current study, within a reaction–diffusion setting, we consider an SIS (susceptible–infected–susceptible) model with a nonlinear incidence rate as in [29,30]. The nonlocal incidence may be attributed to several epidemiological aspects like the behavioral response, saturation effect, heterogeneous mixing of population, crowding effect, etc. Though the empirical data of infectious diseases are insubstantial in several aspects, given a situation, the exact justification of nonlinear incidence rate lies upon the critical understanding of disease transmission mechanism. For example, in an abundance of infected individuals, exposure to the causative agents is more likely and hence less than a linear response could occur due to saturation. In contrast, given a very low density of infected or diseases that requires multiple exposers to transmit, more than a linear response is suitable in modeling prospects. Further, we extend the local model to a nonlocal framework by considering a suitable transmission kernel function. In recent times, a considerable number of studies have been carried out to understand the influence of nonlocal interactions among species of spatio-temporal models. For example, spatio-temporal pattern formation, in the presence of nonlocal interaction in the prey population, has been studied by Pal et al. [31,32]. Their investigation has shown extensive qualitative changes in pattern formation in the presence of nonlocal interaction characterized by various spatial kernels. Further, a generalized version of a three-species cyclic competition model in presence of nonlocal intra-specific competition has been investigated for spatial pattern formation by Manna et al. [33]. Also, a nonlocal interaction between prey and predator has been introduced by Banerjee et al. [34]. Some more recent results concerning the spatio-temporal dynamics due to nonlocal interaction in biological and biomedical models can be found in [35–37]. Nevertheless, the existing literature on the formation of spatio-temporal patterns considers only the local infection between the susceptible and infected populations [38,39]. These models exhibit a variety of both stationary and dynamic patterns. Therefore, a natural question arises regarding the consequences of the nonlocal infection on the formation of spatio-temporal patterns, which is yet to be attempted. It is expected that the presence of nonlocal terms will significantly alter the spatio-temporal dynamics. Our primary objective in this study is to identify these qualitative changes through spatio-temporal asymptotic analysis and discuss the corresponding epidemiological significance. To the best of our knowledge, there does not exist any investigation on the effect of nonlocal disease transmission on spatio-temporal pattern formation. Apart from the asymptotic analysis, we have also discussed the transient dynamics produced by the proposed SIS model. It has been observed that many biological systems undergo a "long transient" before reaching the final state [40–42]. The study of phase transition is essential to understand the sudden change in the dynamics and the presence of ghost attractors. Consequently, it helps in assessing epidemics across human, wildlife, and agricultural systems and designing effective management strategies to combat them [43].

This paper is organized as follows. The temporal SIS model with nonlinear disease incidence term is introduced in Sect. 2 which also discusses the existence of equilibrium points. A complete bifurcation analysis of the temporal model along with graphical visualization for a given dataset is presented in Sect. 3. The temporal model is extended spatially in Sect. 4, where Turing instability of a homogeneous endemic steady state is also discussed. The spatial model is further extended to incorporate the nonlocal disease transmission using a distance transmission kernel in Sect. 5. Here, we have again examined the Turing instability condition of the same endemic steady state. The spatio-temporal patterns exhibited by both the local and nonlocal models are explored with the help of numerical simulations in Sect. 6. The same section also contains the "long transient" behavior exhibited by the system. Finally, we summarize our findings and discuss their epidemiological significance in Sect. 7.

2 Mathematical model

The paradigmatic work of Kermack and McKendrick [1] considers a compartmental epidemic model, known as SIR model, which is a system of coupled ordinary differential equations. Thereafter, many theoretical epidemiologists carried out their investigations in order to study several critical mechanisms of infectious disease transmission and its control. Typical per-capita disease incidence rates, used in most of the epidemic models, are linear in nature. However, it may not be suitable for all the cases and often misses the vital transmission dynamics described by the contagion due to saturation, multiple exposures, inhibition effect followed by the behavioral changes in susceptible, heterogeneous mixing of population, etc. [44,45]. Liu et al. [29,30] described an epidemic model with a nonlinear incidence rate of the form $\beta I^p S^q$, where $\beta, p, q > 0$, and their investigations revealed a wide range of qualitative differences compared to those of epidemic models with standard linear incidence rate. The qualitative dynamics change significantly when p is different from unity. However, the nonlinearity in S does not alter the dynamics qualitatively and it is not epidemiologically justifiable.

Let $S(t)$ and $I(t)$ be the densities of the susceptible and infectious populations, respectively. The model equations are

$$\begin{aligned} \frac{\mathrm{d}S}{\mathrm{d}t} &= \Lambda - \beta S I^2 + \gamma I - \mu S, \\ \frac{\mathrm{d}I}{\mathrm{d}t} &= \beta S I^2 - (\gamma + \sigma + \mu) I, \end{aligned} \tag{1}$$

with non-negative initial conditions $S(0) = S_0$ and $I(0) = I_0$. The parameters of the model are disease transmission rate β, constant recruitment rate to the susceptible population Λ, natural mortality rate of the whole population μ, recovery rate of the infected individual γ, and the disease-induced mortality rate of infected individual σ. Also, it is assumed that recovery does not give any immunity to the disease and hence recovered becomes susceptible to the disease instantaneously.

2.1 Equilibrium points and their stability

System (1) always possesses a disease-free equilibrium point $P_0 = (\frac{\Lambda}{\mu}, 0)$. A co-existing equilibrium point or the endemic equilibrium $P^* = (S^*, I^*)$ satisfies

$$\begin{aligned} &\beta S^* I^* - (\gamma + \sigma + \mu) = 0, \\ &\Lambda - \beta S^* (I^*)^2 + \gamma I^* - \mu S^* = 0. \end{aligned} \tag{2}$$

Eliminating S^* from these two equations, we find

$$a_2 (I^*)^2 + a_1 I^* + a_0 = 0, \tag{3}$$

where $a_2 = \beta(\sigma + \mu)$, $a_1 = -\Lambda\beta$ and $a_0 = \mu(\gamma + \sigma + \mu)$.

For a feasible endemic equilibrium point, we must have a positive root of the quadratic equation (3). Using Descartes' rule of signs, we conclude that the system has either two or zero positive roots. The discriminant of the quadratic equation (3) is given by

$$D = a_1^2 - 4a_0 a_2 = \beta \Lambda^2 (\beta - \beta_c),$$
$$\text{where } \beta_c = \frac{4\mu(\gamma + \sigma + \mu)(\sigma + \mu)}{\Lambda^2}.$$

It is clear that Eq. (3) has two distinct real roots when $\beta > \beta_c$. These two real roots coincide at $\beta = \beta_c$ leading to a unique endemic equilibrium point. Finally, the roots of Eq. (3) are

$$I^*_{1,2} = \frac{\Lambda}{2(\sigma + \mu)} \left(1 \pm \sqrt{1 - \frac{\beta_c}{\beta}} \right).$$

Thus, the endemic equilibria are given by $P^*_{1,2} = (S^*, I^*) = (\frac{\gamma + \sigma + \mu}{\beta I^*_{1,2}}, I^*_{1,2})$. We keep the parameters Λ, μ, γ, σ fixed and choose β as a bifurcation parameter. The Jacobian matrix of system (1) at the endemic equilibrium point (S^*, I^*) is given by

$$\mathcal{J} = \begin{bmatrix} -\beta (I^*)^2 - \mu & -2\beta I^* S^* + \gamma \\ \beta (I^*)^2 & 2\beta I^* S^* - (\gamma + \sigma + \mu) \end{bmatrix}$$

$$\equiv \begin{bmatrix} a_{11} & a_{12} \\ a_{21} & a_{22} \end{bmatrix}. \tag{4}$$

The trace and determinant of the Jacobian matrix are

$$\begin{aligned} &\text{Trace}(\mathcal{J}) = a_{11} + a_{22} = (\sigma + \gamma) - \beta(I^*)^2, \\ &\text{and} \\ &\text{Det}(\mathcal{J}) = a_{11}a_{22} - a_{12}a_{21} \\ &= (\sigma + \mu)\beta(I^*)^2 - (\gamma + \sigma + \mu)\mu. \end{aligned} \tag{5}$$

We need $\text{Trace}(\mathcal{J}) < 0$ and $\text{Det}(\mathcal{J}) > 0$ for local asymptotic stability of the endemic equilibrium point. Further, the equilibrium is a saddle point if $\text{Det}(\mathcal{J}) < 0$.

Proposition 1 *The disease-free equilibrium P_0 is always locally asymptotically stable.*

Proof The Jacobian matrix $\mathcal{J}$ has two negative eigenvalues $-\mu$ and $-(\gamma+\sigma+\mu)$ whenever $I^* = 0$. Therefore, P_0 is always locally asymptotically stable. □

Proposition 2 *The endemic equilibrium point $P_2^* = (S^*, I_2^*)$ is always a saddle point.*

Proof Substituting the expression of $(I^*)^2$ from (3) into (5) and then simplifying, we find

$$\begin{aligned} \text{Det}(\mathcal{J})|_{P_2^*} = \frac{\Lambda^2\beta}{2(\sigma+\mu)}\Bigg[\left(1 - \frac{\beta_c}{\beta}\right) \\ -\sqrt{1 - \frac{\beta_c}{\beta}}\Bigg], \quad \forall\, \beta \geq \beta_c. \end{aligned} \tag{6}$$

Since $0 \leq \left(1 - \frac{\beta_c}{\beta}\right) < 1$, $\forall\ \beta \geq \beta_c$, we conclude that $\text{Det}(\mathcal{J})|_{P_2^*} \leq 0$ whenever $\beta \geq \beta_c$ and the equality occurs only at $\beta = \beta_c$. Therefore, P_2^* is always a saddle point for $\beta > \beta_c$. □

Proposition 3 *The local asymptotic stability of P_1^* depends on the sign of $Trace(\mathcal{J})|_{P_1^*}$.*

Proof The determinant of the Jacobian matrix described in (4) at the endemic equilibrium point $P_1^* = (S^*, I_1^*)$ is

$$\begin{aligned} \text{Det}(\mathcal{J})|_{P_1^*} = \frac{\Lambda^2\beta}{2(\sigma+\mu)}\Bigg[\left(1 - \frac{\beta_c}{\beta}\right) \\ +\sqrt{1 - \frac{\beta_c}{\beta}}\Bigg], \quad \forall\, \beta \geq \beta_c, \end{aligned} \tag{7}$$

which is positive whenever $\beta > \beta_c$. Therefore, the stability of P_1^* depends on the sign of $\text{Trace}(\mathcal{J})|_{P_1^*}$. □

3 Local bifurcation analysis

Model (1) is capable of exhibiting two local bifurcations, namely a saddle-node bifurcation related to the generation of an endemic equilibrium and a Hopf bifurcation related to the destabilization of stable endemicity.

3.1 Saddle-node bifurcation

Proposition 4 *System (1) undergoes a saddle-node bifurcation with respect to the parameter β at the critical point β_c.*

Proof Note that two endemic equilibria collide when $\beta = \beta_c$ leading to a single endemic equilibrium point

$$P_{SN}^* = \left(\frac{\gamma+\sigma+\mu}{\beta_c I_{SN}^*}, I_{SN}^*\right), \qquad \text{where } I_{SN}^* = \frac{\Lambda}{2(\sigma+\mu)}.$$

Further, we observe that $\text{Det}(\mathcal{J}; \beta_c, I_{SN}^*) = 0$. Hence, the Jacobian matrix (4) has a simple zero eigenvalue at P_{SN}^*. Let $\mathrm{v} = (1, \phi)^T$ and $\mathrm{w} = (\psi, 1)^T$ be the left and right eigenvectors corresponding to the zero eigenvalue of the Jacobian matrix at P_{SN}^*. We write that right-hand side of system (1) as $\mathrm{F} = (f, g)^T$ and verify that

$$\begin{aligned} &\mathrm{w}^T \mathrm{F}_\beta(P_{SN}^*; \beta_c) = \frac{\Lambda^2(2\gamma + 3(\sigma+\mu))}{4\mu(\sigma+\mu)(\gamma+2(\sigma+\mu))} \neq 0, \\ &\mathrm{w}^T D^2\mathrm{F}(P_{SN}^*; \beta_c)\mathrm{v} = \gamma + \sigma + \mu \neq 0. \end{aligned}$$

Thus, the transversality conditions of the saddle-node bifurcation are satisfied, and system (1) undergoes a saddle-node bifurcation with respect to the parameter β at $\beta = \beta_c$. □

Remark 1 Unlike other epidemic models, here the endemic equilibrium is generated through a saddle-node bifurcation instead of a transcritical bifurcation.

3.2 Hopf bifurcation

From Proposition 3, it is clear that the endemic equilibrium P_1^* is locally asymptotically stable when $\text{Trace}(\mathcal{J})|_{P_1^*} < 0$. Hence, P_1^* becomes unstable whenever $\text{Trace}(\mathcal{J})|_{P_1^*} > 0$. Hopf-bifurcation threshold is

given by Trace$(\mathcal{J}) = 0$, which on simplification yields a critical value β_h of the parameter β given by

$$\beta_h = \frac{\{(\gamma+\sigma)(\sigma+2\mu)+\mu^2\}^2}{\Lambda^2(\sigma+\gamma)}. \tag{8}$$

Further, it is observed that

$$\text{Det}(\mathcal{J})|_{P_1^*} > 0 \text{ and } \frac{\mathrm{d}}{\mathrm{d}\beta}\left[\text{Trace}(\mathcal{J})|_{P_1^*}\right] \neq 0 \text{ at } \beta = \beta_h. \tag{9}$$

Hence, we arrive at the following proposition:

Proposition 5 *The endemic equilibrium P_1^* undergoes a Hopf bifurcation at $\beta = \beta_h$.*

A limit cycle surrounding the endemic equilibrium $P_1^* = (S_1^*, I_1^*)$ appears near the Hopf-bifurcation threshold $\beta = \beta_h$, and the stability of the bifurcating limit cycle can be determined from the first Lyapunov coefficient $\mathcal{L}_1$. The Hopf bifurcation is supercritical when $\mathcal{L}_1$ is negative at $\beta = \beta_h$ and hence generates a stable limit cycle around the equilibrium point. However, if $\mathcal{L}_1$ is positive at $\beta = \beta_h$, then it generates an unstable limit cycle and the system undergoes subcritical Hopf bifurcation. We shall verify the sign of $\mathcal{L}_1$ with the help of a numerical example.

3.3 Numerical results for the temporal model

Now, we present some numerical simulations of the temporal system (1) to visualize the analytical findings discussed above. We fix the parameter values $\Lambda = 1$, $\mu = 1, \sigma = 1.8, \gamma = 1$ and vary the bifurcation parameter β. Figure 1 illustrates the three different cases of the existence of endemic equilibria. The endemic states appear at the threshold value $\beta = \beta_c \approx 42.56$ via a saddle-node bifurcation and exist for $\beta > \beta_c$. Figure 1 clearly demonstrates that system (1) possesses no endemic equilibrium point for $\beta < \beta_c$. Therefore, an increase in the disease transmission rate β leads to the appearance of the endemic states through a saddle-node bifurcation.

The local and global bifurcations exhibited by system (1) are displayed in Fig. 2. The two branches of equilibria that appear at the saddle-node bifurcation threshold $\beta = \beta_c$ are unstable, and these are shown by the dashed magenta-colored curves. Further, between these two unstable branches of endemic steady states, the one with lesser infected (P_2^*) remains saddle throughout. The other endemic state (P_1^*) emerges as an unstable spiral node and remains the same for $\beta \in (\beta_c, \beta_h) \approx (42.56, 48.39)$. The first Lyapunov coefficient $\mathcal{L}_1$ of the system is positive at $\beta = \beta_h$, and hence, the emerged limit cycle due to the Hopf bifurcation is unstable in nature, shown as dashed blue-colored curves in Fig. 2. Thus, system (1) exhibits a subcritical Hopf bifurcation at $\beta = \beta_h$. Further increment in β increases the amplitude of the unstable limit cycle which finally disappears through a homoclinic bifurcation at $\beta \approx 49.50$. The associated phase portraits of system (1) near the Hopf-bifurcation threshold $\beta = \beta_h$ are illustrated in Fig. 3. Figure 3a shows the phase diagram for $\beta = 49.2 > \beta_h$. The stable and unstable manifolds of the saddle point P_2^* (denoted by a blue dot) are plotted in magenta- and red-colored curves, respectively. The green dot denotes the stable endemic point P_1^* around which the unstable limit cycle is plotted in magenta color. This unstable limit cycle emerges due to subcritical Hopf bifurcation at $\beta = \beta_h$. If we increase β to 49.50, the unstable manifold returns back to the saddle point P_2^* through a homoclinic loop shown in Fig. 3b. Therefore, system (1) undergoes a homoclinic bifurcation at $\beta = 49.50$. Further, the unstable limit cycle disappears for $\beta = 50 > 49.50$ and the unstable manifold of P_2^* converges to both P_1^* and the disease-free equilibrium P_0 as shown in Fig. 3c. It is observed that the basin of attraction of P_1^* is confined inside the unstable limit cycle till the global homoclinic bifurcation at $\beta = 49.50$. But, the stable manifold of P_2^* creates the separatrix between the basin of attractions of the attractors P_0 and P_1^* for $\beta > 49.50$ (see Fig. 3c).

4 The spatio-temporal model

The random movement of the population species can be incorporated by introducing diffusion to the model system (1). A one-dimensional spatial domain $(-L, L)$ is considered with the boundary $\partial\Omega = \{L, -L\}$. The governing equations are

$$\begin{aligned}
\frac{\partial S}{\partial t} &= \Lambda - \beta S I^2 + \gamma I - \mu S + d_1 \frac{\partial^2 S}{\partial x^2}, \\
\frac{\partial I}{\partial t} &= \beta S I^2 - (\gamma+\sigma+\mu) I + d_2 \frac{\partial^2 I}{\partial x^2}, \quad x \in (-L, L),\ t > 0,
\end{aligned} \tag{10}$$

where d_1 and d_2 represent the diffusion coefficients of susceptible and infected species, respectively. The system is subjected to non-negative initial and periodic boundary conditions.

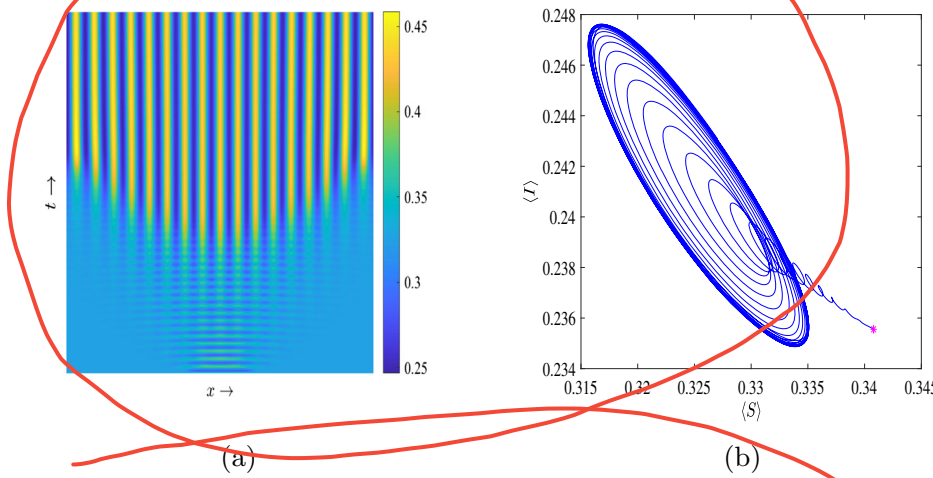

Fig. 14 Transient characteristics of the local system (10) for $\beta = 48.5$ and $d = 2.88$: **a** space–time transient pattern of the infected population, **b** phase diagram of the spatially averaged populations. Other parameter values are given in the caption of Fig. 13. The left panel shows various non-resonant infectious peaks over the spatial domain in the transient state

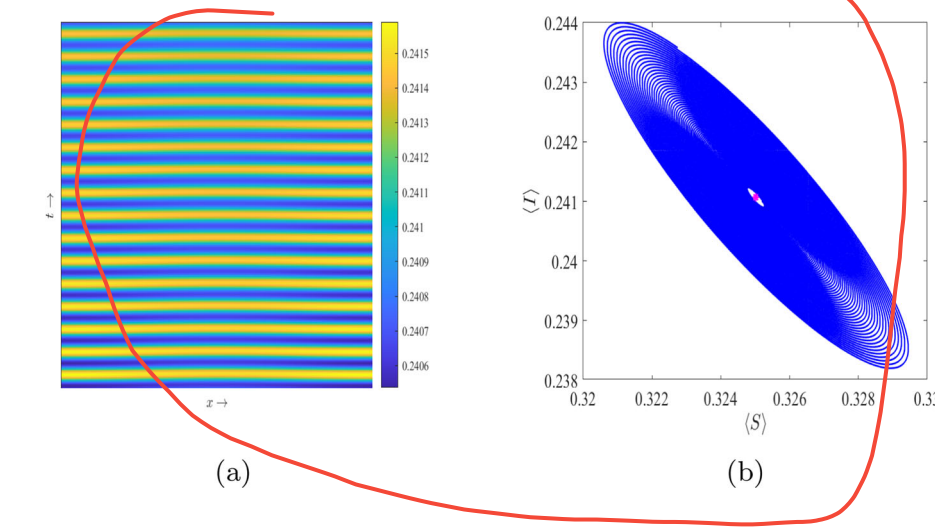

Fig. 15 Transient characteristics of system (10) for $\beta = 48.5$ and $d = 2.5$: **a** space–time transient pattern of the infected population, **b** phase diagram of the spatially averaged populations up to 1200 time unit. Other parameter values are given in the caption of Fig. 13. The left panel depicts multiple epidemic peaks in the transient state of the local system (10)

populations oscillate for a considerable time around the homogeneous steady state (shown by the magenta-colored asterisk in Fig. 15b).

Finally, we analyze the nonlocal system (20) for the transient dynamics using the same initial condition (31). The Turing threshold for $\beta = 48.5$ and $\delta = 0.6$ is $d_1^T \approx 3.531$. Using similar approach as that of the local model, we examine the dependency of the transient duration on the spatial dispersal rate d. In this case, we observed similar transient characteristics as that of the local model (see Fig. 14). It is observed that as d decreases gradually toward d_1^T, system (20) oscillates for a relatively longer duration of time before settling to the stationary spatially heterogeneous solution. The spatial average of the susceptible population against time is plotted for four different values of d in Fig. 16a. It is evident that a higher value of d results in faster convergence to the stationary state of system (20). Further, the nonlocal system exhibits long transient characteristics similar to its local counterpart as d tends to d_1^T from above. The corresponding power law of the transient duration is presented in Fig. 16b.

7 Discussion and conclusions

In the current body of literature, the spatio-temporal dynamics of infectious diseases have been examined considering only the local transmission of the causative agents. The process of disease transmission, however, is not confined to the host's geographic location, and frequently, distant susceptible are at risk of contracting the illness. There are very few studies that model this issue of nonlocal disease spread. As a result, the spatio-temporal dynamics of the disease transmission taking into account the possibility of nonlocal transmission is